Localized Multiphoton Emission of Femtosecond Electron Pulses from Metal Nanotips

C. Ropers,[1] D. R. Solli,[2] C. P. Schulz,[1] C. Lienau,[1,*] and T. Elsaesser[1]

[1]*Max-Born-Institut für Nichtlineare Optik und Kurzzeitspektroskopie, D-12489 Berlin, Germany*

[2]*Los Angeles Department of Electrical Engineering, University of California, Los Angeles, California 90095-1594, USA*

(Received 4 August 2006; published 25 January 2007)

Intense multiphoton electron emission is observed from sharp (~20 nm radius) metallic tips illuminated with weak 100-pJ, 7-fs light pulses. Local field enhancement, evidenced by concurrent nonlinear light generation, confines the emission to the tip apex. Electrons are emitted from a highly excited nonequilibrium carrier distribution, resulting in a marked change of the absolute electron flux and its dependence on optical power with the tip bias voltage. The strong optical nonlinearity of the electron emission allows us to image the local optical field near a metallic nanostructure with a spatial resolution of a few tens of nanometers in a novel tip-enhanced electron emission microscope.

DOI: 10.1103/PhysRevLett.98.043907 PACS numbers: 42.70.Qs, 07.79.Fc, 42.25.−p, 73.20.Mf

Femtosecond electron and x-ray diffraction and imaging are currently among the most intriguing topics in ultrafast science, allowing the microscopic structural dynamics of molecular and solid state systems to be probed with previously unachievable spatiotemporal resolution [1–4]. Despite substantial recent progress, these experimental techniques are still in an early stage, and large efforts are currently devoted to the development of sophisticated femtosecond electron [5] and x-ray [6] sources suitable for experiments with high temporal resolution. In ultrafast electron diffraction and microscopy [7,8], overcoming temporal smearing due to spatial propagation effects and to Coulomb repulsion of electron bunches produced at kilohertz repetition rates is particularly challenging. Therefore, it would be desirable to use *individual* nanostructures as quasipointlike sources of single electrons with a sub-10-fs time structure.

For such purposes, metallic nanoantennas, e.g., sharp gold tips, have promising properties. Fabricated with structure sizes of about 10 nm, they offer large optical field enhancement and high damage thresholds. So far, however, little is known about the microscopic physics underlying femtosecond electron emission from metal nanotips. Very recently, photoinduced electron emission from sharp metal tips following femtosecond laser excitation has been demonstrated at high kilovolt bias voltages [5]. Electron generation was attributed to one-photon-assisted tunneling or—for blunt tips and higher intensities—to optical field emission. Such high bias voltages prevent direct use of such tips for nanoimaging.

In this Letter, we demonstrate, by illuminating ultrasharp metal tips with light pulses of sub-10-fs duration, intense electron emission from a pointlike area at the tip apex, even in the absence of bias voltages. Our experiments show that electrons are generated from a short-lived nonequilibrium carrier distribution and that different parts of this distribution function are emitted depending on the bias voltage. The generation mechanism changes from one-photon-assisted tunneling at high bias voltages to four-photon-induced emission at zero bias. This strong nonlinearity makes the electron signal sensitive to the local field at the tip apex, as is shown by imaging a metallic nanostructure with a spatial resolution of a few tens of nanometers in a novel tip-enhanced electron emission microscope.

Our experimental setup is schematically shown in Fig. 1(a). An electrochemically etched metal tip, e.g., from gold or tungsten, with a radius of curvature of about 20 nm is mounted on a piezoscanner inside a high-vacuum chamber. Light pulses from an 80 MHz Ti:sapphire oscillator with a center wavelength of 800 nm and a duration of 7 fs enter through a thin quartz window and are focused onto the tip to a spot size of $\sim 1\ \mu\mathrm{m} \times 2\ \mu\mathrm{m}$ using a Cassegrain mirror objective. The light polarization is along the z axis, i.e., parallel to the tip. Electrons emitted from the tip are detected with a microchannel plate opposing the tip and are counted with an electronic discriminator. The scattered light is collected in a backreflection geometry, spectrally resolved, and detected with a cooled charge coupled device camera. The piezoscanner allows us to raster scan the tip through the laser focus, while the electron emission and the spectrally resolved light scattering are recorded simultaneously. The experiments are performed for tip bias voltages between 0 and 1000 V.

Illuminating a sharp metal tip with femtosecond light pulses results in nonlinear frequency conversion [9–11]. The generated light is composed of the second harmonic of the laser pulses ($\approx$ 400 nm) and a broad continuum in the range between 450 and 700 nm [10]. Local field enhancement at the apex of the metal tip localizes the nonlinear light generation at the very end of the tip. This spatial localization is directly seen in Fig. 1, comparing images of the linearly scattered laser light [Fig. 1(b)] and the light generated in the wavelength range between 400 and 600 nm [Fig. 1(c)]. In these images, the tip is scanned through the laser focus in the x-z plane perpendicular to the optical axis. Its spot size, here about $0.8\ \mu\mathrm{m} \times 1.5\ \mu\mathrm{m}$, is given only by the spatial shape of the laser focus, which is

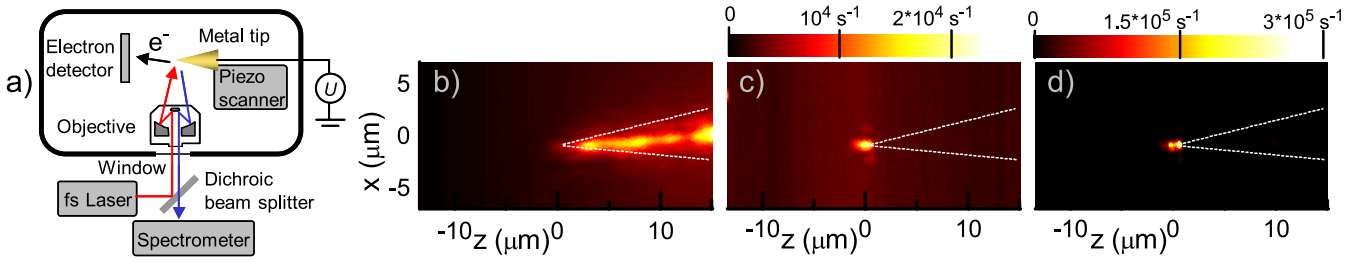

FIG. 1 (color online). (a) Experimental setup. (b) Spatial scan of the fundamental laser light backscattered from a sharp gold tip (lines). (c) Nonlinear light generation localized at the very end of the tip. (d) Simultaneous electron emission. (Images at $U = 0$.)

also responsible for the weak sidelobes above and below the peak position. Figure 1(d) shows the simultaneously recorded electron signal. We find intense emission of electrons generated at exactly the same position as the frequency-converted light; i.e., local field enhancement is responsible for both electron emission and optical frequency conversion. In the electron image, taken at 0 V, the spot size is further reduced to about 0.6 μm $\times$ 1.1 μm. For illumination with 150-pJ pulses at 80 MHz, a total electron flux of up to 10^7 s^{-1} is detected at zero tip bias, corresponding to somewhat less than 1 electron per laser pulse. Such very low optical pulse energies correspond to a laser fluence of ≈ 7 mJ/cm^2 in the laser focus, well below the damage threshold of gold. The weak signals from the shaft of the tip in Figs. 1(c) and 1(d) indicate that both nonlinear frequency conversion and electron emission originate from an area of a size determined by the curvature of the tip. This shows that local field enhancement, together with the strong nonlinear nature of the light-matter interaction, is essential for the free electron generation. This enhanced susceptibility at the metallic tip is highly directional along the tip axis. For polarization perpendicular to this axis, electron emission is suppressed by more than 2 orders of magnitude.

Comparing the electron flux from the tip apex with that from the shaft (cf. Fig. 1), one can estimate a local electric field enhancement with respect to the incoming laser field of $\alpha = |E_{\mathrm{loc}}/E_0| = 10$. The corresponding enhancement factor for nonlinear frequency conversion has a value of $\alpha = 15$. These numbers are in rather good agreement with theoretically predicted values ($\alpha \approx 12$) for gold tips of similar sharpness [9].

To gain insight into the microscopic mechanisms underlying electron emission, we studied the electron flux as a function of intensity and tip bias voltage. At zero tip bias, we obtain a fourth-order dependence of the electron signal J on the incident laser power P [Fig. 2(a)]. The inset in Fig. 2(a) shows the electron signal generated by a pair of phase-locked laser pulses as a function of the pulse delay (interferometric autocorrelation), and a strong enhancement of the electron flux is found at zero delay. At zero bias, only electrons excited to states above the vacuum level can be emitted from the tip (work function of gold $\simeq$5 eV), and the clear fourth-order power dependence directly points to the absorption of four laser photons of about 1.5 eV energy each. Upon application of a negative tip bias voltage, we observe a strong increase of the background generated by dc field emission for voltages above 400 V and, most importantly, a much weaker dependence of the generated electron flux on the incident laser power. At 880 V, the electron flux is only slightly nonlinear with a power dependence $\propto P^{1.4}$ around $P = 3$ mW. At these high bias voltages, the multiphoton electron emission is complemented by tunneling from lower-lying electron states, which plays an increasingly important role with increasing bias. In Fig. 2(b), this tunneling scheme is depicted schematically. Even without illumination, i.e.,

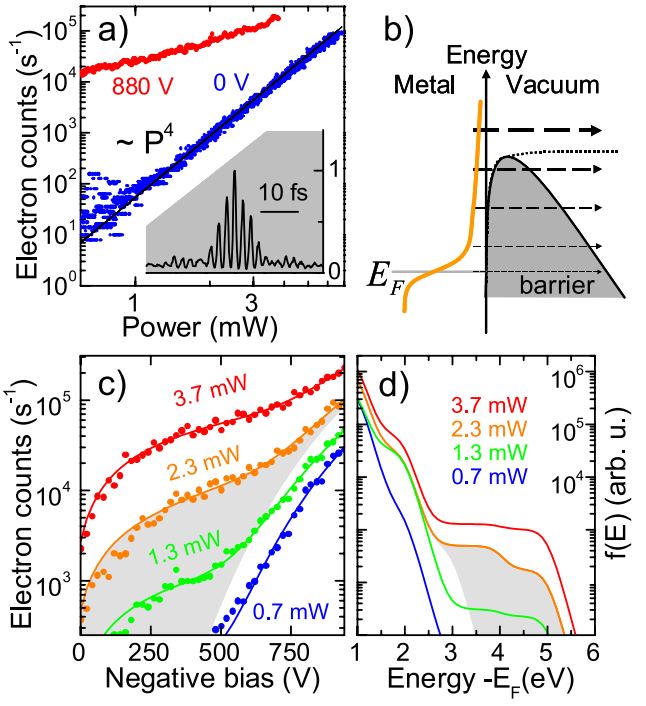

FIG. 2 (color online). (a) Power dependence of the electron signal for bias voltages of 0 and 880 V. Inset: Interferometric autocorrelation of the laser pulses detected via the electron signal. (b) Illustration of the tunneling model. (c) Voltage dependence of the electron emission for four different incident powers and predicted currents from the inferred nonequilibrium carrier distributions shown in (d).

for an electron distribution at a temperature of 300 K, electrons from states close to the Fermi energy tunnel into the vacuum, a process made possible by the dc field enhancement at the tip apex. Analyzing the voltage dependence of this emission using the Fowler-Nordheim equation indicates an electric field of $\approx 10^{-2}$ V/nm per volt tip bias.

In order to obtain a more detailed understanding of the observed effects, we have measured the voltage- and power-dependent electron flux $J(U, P)$ in small steps. In Fig. 2(c), the voltage-dependent electron emission is displayed for four different incident powers (circles). The gradual decrease of the power dependence from a fourth-order nonlinearity at low bias voltages towards linear emission at high voltages is evident in the decreasing separation between the curves (logarithmic scale) with increasing voltage. The femtosecond excitation of the gold tip generates a transient carrier distribution with a pronounced population well above the Fermi energy [12,13]. For a given tip, the voltage-dependent electron flux $J(U, P)$ at a particular optical power P carries information on the underlying energy distribution of excited carriers. In an extension of the conventional Fowler-Nordheim approach, $J(U, P)$ is given by an integral over the energy- and voltage-dependent transmission coefficients $S(E, U)$ times a distribution function of the optically excited carriers $f(E, P)$:

$$J(U, P) \propto \int_0^\infty dE S(E, U) f(E, P). \quad (1)$$

Here the emission probability $S(E, U)$ of a state at energy E for a bias voltage U is calculated from a standard WKB treatment, taking the known surface electric field of the tip into account. As $S(E, U)$ is a known function for the characterized tip, it is possible to reconstruct from the measured $J(U, P)$ the underlying optically excited distribution functions $f(E, P)$. This function is a time average over the transient nonequilibrium electron distribution during the course of the emission process. We have performed this reconstruction by discretizing Eq. (1) with respect to U and E, leading to a matrix equation $J(U_i, P) = \sum_j S(E_j, U_i) f(E_j, P)$. Least squares solutions for $f(E, P)$ were calculated numerically by minimizing the error functional $\varepsilon = J(U, P) - S(E, U) f(E, P)$. This reconstruction is shown in Fig. 2(d) for the same incident powers as in Fig. 2(c). The solid lines in Fig. 2(c) are in excellent agreement with the experimental results and represent the electron currents resulting from these distributions.

The distribution functions possess a markedly nonthermal character and are composed mainly of two components: (i) a strong low-energy component close to the Fermi energy which originates from single-photon absorption (its energy content scales linearly with the incident optical power) and (ii) a nonthermal high-energy shoulder which emerges between 3 and 6 eV [indicated by the gray-shaded area in Fig. 2(d) for $P = 2.3$ mW] with a strong nonlinear power dependence, resulting from multiphoton absorption from states below and up to the Fermi energy. The large spectral width of the excitation pulses and the fast decoherence of the generated optical polarization cause an additional energy broadening. It is this second component in the distribution functions which is responsible for the emission at low bias voltages, as is illustrated by the large gray-shaded area in Fig. 2(c) that corresponds to emission from the shaded area in the distribution function in Fig. 2(d). Although a substantial electron emission is already present at zero bias voltage, there is a sharp rise in electron flux upon increasing the bias from 0 to 100 V. This fact suggests that the major fraction of the nonthermal component populates states somewhat below the vacuum level.

The strong nonthermal character of the electron distributions has direct consequences for the time structure of the emitted electrons. For low voltages, the sub-20-fs thermalization of electrons limits the population lifetime of the relevant high-energy states [14,15] and, thus, the duration of the emitted electron pulses. With increasing negative bias, lower-lying states of longer lifetime [16] contribute significantly, resulting in longer pulses.

A comment should be made on Keldysh-type [5,17] optical field emission from the Fermi energy potentially occurring because of the high electric fields of the excitation pulses. In our experiments, despite the short laser pulses and the substantial field enhancement $\alpha \simeq 10$ at the metal tip (see above), we estimate a Keldysh parameter $\gamma = \sqrt{\Phi/2U_p} \simeq 4$ at $P = 3$ mW. Here Φ is the work function and $U_p = e^2\alpha^2 E_0^2/(4m_e\omega^2)$ the ponderomotive potential (E_0: incident field; ω: laser frequency). We thus expect that the present experiments are well into the multiphoton regime [18]. This is supported by finding the same fourth-order power dependence for various tips at zero bias, whereas optical field emission should strongly depend on the local field enhancement and thus vary from tip to tip.

The high optical nonlinearity of the electron emission in the absence of a bias voltage makes such nanotips exceptionally sensitive to probing local electromagnetic fields through a modification of the free electron yield. To explore this potential, we have set up a novel tip-enhanced electron emission microscopy (TEEM) [19]. The setup, based on a mechanically durable tungsten tip in proximity to a nanostructured gold surface (a 100 nm wide groove [20]), is displayed in Fig. 3(a). In order to verify both surface sensitivity and lateral resolution of this setup, we illuminate tip and sample with focused 7-fs light pulses and monitor the locally generated electron flux while raster scanning the sample position relative to the tip in the x-z plane, i.e., perpendicular to the sample surface. Specifically, approach curves in the z direction are recorded by moving the sample back and forth for every position along the x direction. The approach is reversed

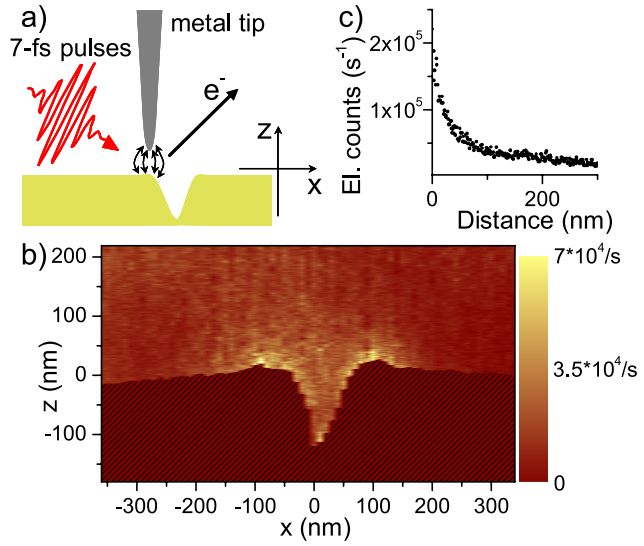

FIG. 3 (color online). (a) TEEM setup. The illuminated metal tip is brought close to a nanostructure, and the local electron generation rate is monitored as the sample position is scanned relative to the tip. (b) Distance-dependent TEEM image of a nanometric groove in a gold surface. The cross section of the groove is given by the shaded area and determined by AFM measurement. (c) Electron signal approach curve near a groove edge.

whenever force contact (monitored via a shear-force setup) is established. These contact points provide a topographic image of the sample surface, similar to an atomic force microscopy (AFM) scan, as shown by the dark area in Fig. 3(b). The color-coded image of Fig. 3(b) on the air side of the metal surface represents the local electron signal as a function of the relative tip-sample position. It is evident that the electron signal is strongest when the tip is in direct vicinity of the sample surface and close to the edges of the groove. An approach curve near a groove edge [Fig. 3(c)] shows an increase of the electron signal by a factor of ~ 5 within the last 50 nm to the surface. In the lateral x direction, the spatial resolution is clearly better than 40 nm and most likely limited only by the sharpness of the tip and the nanostructure features. These results show directly that the electron signal is predominantly generated in the gap between tip and sample and that the spatial resolution of this microscope is thus given by the size of the metal tip and not by the wavelength of the illuminating light.

In more detail, this behavior is understood when considering the near-field distribution at such an illuminated nanometer-scale slit. In diffraction from an ideal rectangular slit, it is known [21] that the electric field component polarized along the z direction, i.e., along the tip axis, diverges near the slit edges, giving rise to strong field localization. Although the slit in the present sample has a rounded cross section, this field localization is still pronounced, leading to the strong increase in local electron yield near the groove edges. This demonstrates that the tip-enhanced electron emission indeed images, in a nonlinear way, the z component of the local electric field. It is easily envisaged that such a TEEM microscope—when illuminated with pairs of time-delayed femtosecond pulses—could analyze, for example, the time dynamics of surface polariton wave packets in metallic [22] and also nonconducting nanostructures.

In conclusion, we have demonstrated localized femtosecond electron emission from a single metal nanoemitter tip that is based on a local enhancement of the optical driving field and accompanied by nonlinear light generation. The experiments give clear evidence for electron emission from a highly excited nonthermal carrier distribution, resulting in a pronounced variation of the effective nonlinear order of the emission process with tip bias voltage. Our pointlike electron source allows for various forms of imaging on a nanometer scale by a sample-induced variation of the electron emission, as shown here, or by electron diffraction from a sample.

Financial support by the DFG (SFB 296) is gratefully acknowledged. We thank J. R. Dwyer, M. J. Lisowski, and T. Kampfrath for helpful discussions and D. S. Kim for providing the metal nanostructures.

*Present address: Carl von Ossietzky Universität Oldenburg, Institut für Physik, 26111 Oldenburg, Germany. Electronic address: christoph.lienau@uni-oldenburg.de

[1] H. Ihee *et al.*, Science **291**, 458 (2001).
[2] B. J. Siwick *et al.*, Science **302**, 1382 (2003).
[3] M. Bargheer *et al.*, Science **306**, 1771 (2004).
[4] A. M. Lindenberg *et al.*, Science **308**, 392 (2005).
[5] P. Hommelhoff *et al.*, Phys. Rev. Lett. **96**, 077401 (2006).
[6] N. Zhavoronkov *et al.*, Opt. Lett. **30**, 1737 (2005).
[7] V. A. Lobastov, R. Srinivasan, and A. H. Zewail, Proc. Natl. Acad. Sci. U.S.A. **102**, 7069 (2005).
[8] W. E. King *et al.*, J. Appl. Phys. **97**, 111101 (2005).
[9] A. Bouhelier *et al.*, Phys. Rev. Lett. **90**, 013903 (2003).
[10] M. R. Beversluis, A. Bouhelier, and L. Novotny, Phys. Rev. B **68**, 115433 (2003).
[11] M. Labardi *et al.*, Opt. Lett. **29**, 62 (2004).
[12] J. G. Fujimoto *et al.*, Phys. Rev. Lett. **53**, 1837 (1984).
[13] W. S. Fann *et al.*, Phys. Rev. Lett. **68**, 2834 (1992).
[14] M. Aeschlimann, M. Bauer, and S. Pawlik, Chem. Phys. **205**, 127 (1996).
[15] H. Petek and S. Ogawa, Prog. Surf. Sci. **56**, 239 (1997).
[16] J. J. Quinn, Phys. Rev. **126**, 1453 (1962).
[17] L. V. Keldysh, Sov. Phys. JETP **20**, 1307 (1965).
[18] S. I. Anisimov, V. A. Benderskii, and G. Farkas, Sov. Phys. Usp. **20**, 467 (1977).
[19] M. I. Stockman and P. Hewageegana, Nano Lett. **5**, 2325 (2005).
[20] C. Ropers *et al.*, Phys. Rev. Lett. **94**, 113901 (2005).
[21] C. J. Bouwkamp, Philips Res. Rep. **5**, 321 (1950).
[22] A. Kubo *et al.*, Nano Lett. **5**, 1123 (2005).